Meaning of xylan acetylation on xylan-cellulose interactions: A quartz crystal microbalance with dissipation (QCM-D) and molecular dynamic study

Zahraa Jaafar, Karim Mazeau, Alexandre Boissière, Sophie Le Gall, Ana Villares, Jacqueline Vigouroux, Nadège Beury, Céline Moreau, Marc Lahaye, Bernard Cathala

Meaning of xylan acetylation on xylan-cellulose interactions: a quartz crystal microbalance with dissipation (QCM-D) and molecular dynamic study

Zahraa Jaafar[1], Karim Mazeau[2], Alexandre Boissière[1], Sophie Le Gall[1], Ana Villares[1], Jacqueline Vigouroux[1], Nadège Beury[1], Céline Moreau[1], Marc Lahaye[1], Bernard Cathala[1*]

[1]: INRA, BIA, 44300 Nantes, France

[2]: Univ. Grenoble Alpes, CNRS, CERMAV, 38000 Grenoble, France

*Corresponding author: bernard.cathala@inra.fr

***To whom correspondences should be addressed:** bernard.cathala@inra.fr

Fax: 00 33 (0) 2 40 67 50 68

Other authors' email addresses:

zahraa.jaafar@inra.fr; karim.mazeau@cermav.cnrs.fr; alexandre.boissiere@inra.fr; sophie.le-gall@inra.fr; ana.villares@inra.fr; jacqueline.vigouroux@inra.fr; nadege.beury@inra.fr; celine.moreau@inra.fr; marc.lahaye@inra.fr;

ABSTRACT

In plant cell walls, xylan chains present various substituents including acetate groups. The influence of the acetyl substitution on the organization of xylan-cellulose complexes remains poorly understood. This work combines *in vitro* and *in silico* approaches to decipher the functional role of acetyl groups on the xylan/cellulose interaction. Acetylated xylans were extracted from apple pomace with dimethyl sulfoxide-lithium chloride (DMSO-LiCl) and deacetylated using a mild alkali treatment. The adsorption behavior of acetylated and deacetylated xylan fractions was investigated using quartz crystal microbalance with dissipation (QCM-D) and molecular dynamics. Acetylated xylans form a dense and poorly hydrated and rigid layer on cellulose with xylan chains that have two residues per helical turn conformation, whereas the deacetylated fraction forms a swollen and more viscous layer in which only the xylan chains in direct contact with the cellulose surface have two residues per helical turn conformation. The other chains have three residues per turn conformation.

Keywords:

Xylan; acetyl group; cellulose nanocrystal; quartz crystal microbalance with dissipation (QCM-D); molecular dynamics; hemicellulose.

Graphical abstract

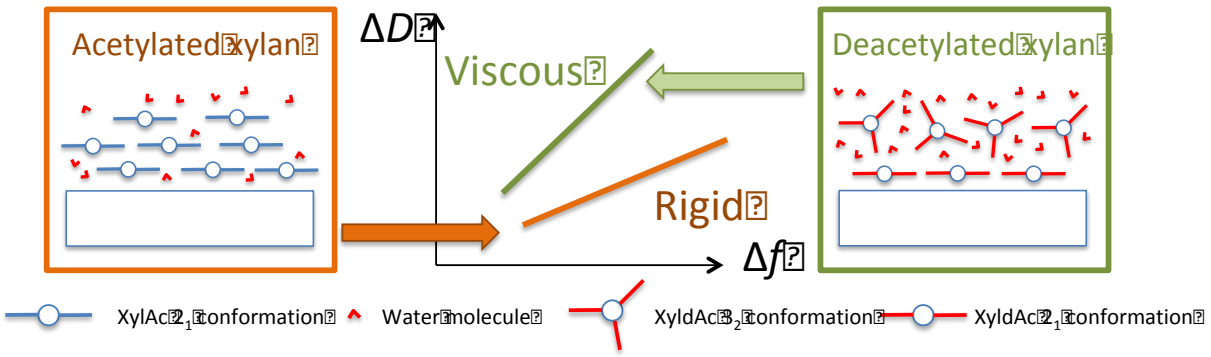

INTRODUCTION

Plant cell walls are highly complex materials that consist of an intricate network of biopolymers whose main components are polysaccharides. These components include cellulose, pectin and hemicellulose. As a result of their many uses, their structure and function *in planta* has been the focus of many studies (Rojas, 2016; Voragen, Schols, & Visser, 2003). Hemicellulose represents a group of various polysaccharides traditionally extracted by alkaline treatment from plant cell walls. These polysaccharides in dicots are based on a β-(1-4) linked backbone of xylose or glucose and/or mannose, forming xyloglucan, xylan, mannan and glucomannan families (Scheller & Ulvskov, 2010). They exhibit large variations in composition and structure depending on their botanical origin, tissue type and developmental stage. This is particularly true of their backbone substitutions with side chains of saccharide units, hydroxycinnamic acids, methyl ether and acetyl ester groups (Brummell & Schröder, 2009; Gatenholm & Tenkanen, 2004; Scheller & Ulvskov, 2010). Specific substitution patterns and their role *in planta* remain unclear. Acetyl esterification is a ubiquitous substitution within hemicellulose families. It usually occurs on O-2 and/or O-3 of xylose in xylan, on O-6 of galactose and/or mannose, and O-2 and/or O-3 of mannose in mannan/glucomannan (Melton, Smith, Ibrahim, & Schröder, 2009; Sims, Craik, & Bacic, 1997), and on fucose and/or O-6, O-4 or O-3 of galactose in xyloglucan, although the exact position has yet to be fully established (Quemener et al., 2015; York, Oates, van Halbeek, Darvill, & Albersheim, 1988). The alteration of xylan acetyl esterification *in planta* severely impacts the plant phenotype and its resistance to biotic stresses (Escudero et al., 2017; Grantham et al., 2017; Kumar, Campbell, & Turner, 2016; Yuan, Teng, Zhong, & Ye, 2016). From the applied point of view, decreasing xylan acetyl esterification improves enzymatic

saccharification in the lignocellulosic biomass biorefinery (Kumar et al., 2016; P. M. Pawar et al., 2016).

Accordingly, understanding the role of the hemicellulose structure in terms of its interactions with cellulose and its consequences on cell wall architecture and properties remains a key question in plant development and applications. The present study focuses on the role of acetyl ester decorations on xylan interactions with cellulose by combining *in vitro* and *in silico* experiments to assess the adsorption features of acetylated and deacetylated xylans.

In the case of *in vitro* experiments, a major challenge is the availability of unmodified xylan fractions since acetyl esters are lost when using classical alkaline hemicellulose extractions. However, acetylated xylans can be recovered from wood biomass using DMSO extraction, steam explosion or organosolv pulping (Gatenholm & Tenkanen, 2004). In rich primary cell wall biomass such as fleshy fruit, acetyl-esterified hemicellulose is recovered after the partial removal of pectin in the cell wall via dimethyl sulfoxide doped by lithium chloride (DMSO-LiCl) (Assor, Quemener, Vigouroux, & Lahaye, 2013; Ray, Vigouroux, Quemener, Bonnin, & Lahaye, 2014).

In this study, interactions of acetylated and deacetylated xylan-enriched fractions obtained by this approach from apple pomace were assessed on a cellulose model surface using quartz crystal microbalance and dissipation (QCM-D). QCM-D is a highly effective mass-sensing technique based on the piezoelectric properties of quartz crystals. It has been successfully used to monitor the hemicellulose adsorption on the cellulose nanocrystal model surface. In fact, it provides information about the mass adsorbed on the surface as well as the mechanical behavior of the layer through the measurement of the dissipation factor (Benselfelt et al., 2016; Eronen, Osterberg, Heikkinen, Tenkanen, & Laine, 2011; Kohnke, Ostlund, & Brelid, 2011; Villares, Bizot, Moreau, Rolland-Sabate, & Cathala, 2017; Villares, Moreau, Capron, & Cathala, 2014; Villares, Moreau, Dammak, Capron, & Cathala, 2015). Recently, Villares et

al. reported the kinetically-driven xyloglucan adsorption on the cellulose surface and described a two-regime mechanism (Villares et al., 2015). A similar approach was applied to investigate the adsorption behavior of acetylated and deacetylated xylan-enriched fractions referred to as XylAc and XyldAc, respectively, which display different behaviors. As a complement to the *in vitro* experiment, molecular dynamics (MD) were used to explore the conformation of xylan chains at the surface of cellulose crystals and to assess their interactions with water.

MATERIAL AND METHODS

Chemicals

Dimethyl sulfoxide (DMSO), lithium chloride (LiCl), 37% hydrochloric acid (HCl), orcinol, standard monosaccharides, sodium tetraborate, 1-methylimidazol, acetic anhydride, sodium borohydride, ammonia 25%, hydrogen peroxide and dichloromethane were provided by Sigma-Aldrich Chimie (Saint-Quentin Fallavier, France). Poly(allylamine hydrochloride) (PAH) was purchased by PolySciences (Mw 120-200 000 g mol-1; sodium hydroxide (50%) (NaOH) by Fluka (Sigma-Aldrich Chimie, Saint-Quentin Fallavier, France); m-hydroxydiphenyl (MHDP, 3 phenylphenol) by Acros Organics (Geel, Belgium); sulfuric acid by Fisher Scientific, Illkirch, France; and ethanol 99% by VWR (Fontenay-sous-Bois, France).

Cellulose Nanocrystal (CNC) Suspension

Cellulose nanocrystals (CNCs) were obtained by sulfuric acid hydrolysis of cotton linters according to Revol et al. (Revol, Bradford, Giasson, Marchessault, & Gray, 1992). Cotton linters were hydrolyzed with 65% wt H_2SO_4 at 65°C for 35 min (12 g cotton linters/170 mL H_2SO_4). Immediately following hydrolysis, the suspension was diluted 10-fold to stop the

reaction and then washed by centrifugation at 10000 rpm for 10 min in order to concentrate the cellulose and to remove the excess aqueous acid. The resulting precipitate was repeatedly rinsed with ultrapure water and recentrifuged until a colloidal suspension was obtained. The colloidal suspension was then dialyzed again with distilled water until neutrality (dialysis membranes MWCO 12-14kDa, Fisher Scientific), after which a mixed-bed research-grade resin (1 g resin/400 g CNC suspension; Sigma-Aldrich TMD-8) was added to the suspension for 48 h to remove residual ions. The final aqueous suspension was 2% concentration by weight (~45% yield). The average crystal dimensions (length and cross-section) measured by tapping-mode atomic force microscopy (AFM) were 100-200 nm x 6-8 nm. Charges determined by conductometric titration were equal to 0.098 e/nm^2.

Hemicellulose extraction

Native hemicellulose enriched fractions were sequentially extracted from apple pomace obtained from the "Institut Français des Produits Cidricoles" (IFPC, Le Rheu, France), according to the procedure described by Ray et al. (Ray et al., 2014). First, the pectin was partially extracted from fresh apple pomace (15.6 kg) with 37.5 L of a potassium oxalate solution (60 mM, pH 4.7, 16 h) at room temperature (~20 °C) and with 3 x 24 L of water (2 x 3 h and 16 h) at 80 °C. After each extraction, the insoluble residue was recovered by manually pressing through a nylon mesh. The final residue was freeze-dried, weighed and ground (yield: 79% initial DW). The insoluble residue (200 g) was then incubated with 4 L of DMSO-LiCl (8.4 wt%; 5 h at 100 °C) under gentle agitation and nitrogen flow. After centrifugation (11000 g, 15 min, 20 °C), the supernatant was evaporated to dryness using a rotary evaporator at 70 °C and the dried residue was dissolved in 300 mL of water. Native hemicellulose was then precipitated with four volumes of ethanol at 4 °C for 16 h. After centrifugation (11000 g, 15 min, 20 °C), the dried pellet was weighed and the yield of

DMSO-LiCl extraction was calculated as 5% initial DW. Sixteen g of native hemicellulose were fractionated by anion exchange chromatography (DEAE- Sepharose Fast Flow column, 5 cm × 15 cm, GE Healthcare, Uppsala, Sweden) (Ray et al., 2014). Elution was performed at a flow rate of 2 mL min^{-1} with water (two column volumes, 600 mL) to recover the unbound fraction. Bound polysaccharides were eluted using a gradient (six column volumes) from 0 to 1.0 M NaCl. XylAc was recovered in the second carbohydrate eluting peak (~400 mL elution, ~0.25 M NaCl) determined by colorimetry (see below), dialyzed and freeze-dried (yield: 500 mg, i.e., 0.14% initial DW). An additional removal of pectin was then performed by pectin lyase (0.12 U, 3 h at 40 °C, [EC 4.2.2.10] purified from Peclyve Lyven, France) (Ralet et al., 2012). The XylAc fraction (100 mg) was deacetylated by saponification with 20 mL of 0.5 M NaOH (1 h at 4 °C). After neutralization with HCl, the deacetylated fraction, referred to as XyldAc, was desalted by dialysis against deionized water (MWCO 3500 Da, CelluSep H1) and freeze-dried in order to obtain (the yield is greater than 90% DW of the XylAc fraction).

Hemicellulose characterization

The total neutral sugar content was determined by colorimetry with an automated orcinol/sulfuric acid assay (Tollier & Robin, 1979). Glucose was used as a standard.

Uronic acid content was measured by colorimetry using m-hydroxydiphenyl and concentrated sulfuric acid hydrolysis (Blumenkrantz & Asboe-Hansen, 1973; Thibault, 1979). The distinction between galacturonic acid and glucuronic acid was made by comparing colorimetric responses with and without the addition of sodium tetraborate in the acid, according to the procedure used by Filisetti-Cozzi, & Carpita (1991). Galacturonic and glucuronic acids were used as the standard.

Identification and quantification of neutral sugars were performed by gas-liquid chromatography on a TG-225 GC Column (30 x 0.32 mm ID) using a TRACE™ Ultra Gas Chromatograph (Thermo Scientific™; column temperature: 205 °C; split injector temperature: 220 °C; flame ionization detector temperature: 250 °C; carrier gas: H^2) after sulfuric acid degradation and derivatization as alditol acetates (Dheilly et al., 2016).

Acetyl ester content was measured by HPLC as the amount of acetic acid released by saponification of a 5-mg sample in 1 mL 0.5 M NaOH for 1 h at 4 °C. HPLC was carried out on a C18 column (4 mm × 250 mm, Lichrospher 100 RP-18e (5 µm), Interchim, France) thermostated to 25 °C using a refractometric detector (Waters, 2414). An isocratic elution of 4 mM H_2SO_4 was used at a flow rate of 1.0 mL min^{-1} (Levigne, Thomas, Ralet, Quemener, & Thibault, 2002).

Surface preparation

Piezoelectric AT-cut quartz crystals coated with gold electrodes on each side (QSX301, Q-Sense) were used for QCM-D experiments. Silicon wafers were used for AFM experiments. Quartz crystals and silicon wafers were cleaned with H_2SO_4/H_2O_2 (7:3, v/v), rinsed exhaustively with Milli-Q water, and dried under a nitrogen stream. Prior to use, QCM-D quartz sensors were subjected to a plasma-etching device (Harrick Plasma). CNC surfaces on quartz crystals were prepared by the spin-coating method, as previously described (Villares et al., 2015). A CNC dispersion at 3 g L^{-1} was dropped onto a pre-coated substrate with poly(allylamine hydrochloride) at 1 g L^{-1} in water and accelerated from 180 rpm to 3600 rpm after 5 min of adsorption and maintained for 60 s at that speed using an expressly designed spin-coater. The thickness of the CNC layer, evaluated by ellipsometry, was 9 nm ± 5 nm, in agreement with previous reports (Villares et al., 2017; Villares et al., 2015). Xylan solutions

187 at 1 g L^{-1} were then dropped onto wafers pre-coated with CNCs in order to perform AFM
188 experiments.
189
190 *Quartz crystal microbalance with dissipation (QCM-D) experiments*
191 QCM-D experiments were carried out using a Q-Sense E4 instrument (AB, Sweden). Spin-
192 coated CNC surfaces were mounted in the QCM-D cells at 20 °C and equilibrated with water
193 at a flow rate of 50 µL min^{-1} until the resonance response was stable. The frequency and
194 dissipation signals were then offset to zero just before the measurement.
195 Frequency ($\Delta f_n/n$) and dissipation (ΔD_n) changes were simultaneously registered at 5 MHz
196 fundamental resonance frequency (n = 1) and its several overtones as a function of time (n =
197 3, 5, 7, etc.). The third overtone (15 MHz, n = 3) was used to evaluate the QCM-D data.
198 Xylan solutions at different concentrations (0.3 to 20 µg mL^{-1}) were injected at 50 µL min^{-1}
199 and allowed to adsorb for 40 min before being exposed again to a water flow in order to
200 remove loosely-bound material. Each xylan solution at the desired concentration was
201 adsorbed on a freshly-prepared CNC modified surface and the experiments were repeated at
202 least three times. All QCM-D experiments were conducted at a constant temperature of 20 °C.
203 The surface concentration (Γ) can be calculated from the mass variation during adsorption
204 obtained from the frequency change ($\Delta f_n/n$) by using the Sauerbrey equation (Sauerbrey,
205 1959):

206 $$\Delta m = -C\frac{\Delta f_n}{n}$$

207 where C is the Sauerbrey constant: constant for the mass sensitivity of the quartz crystal
208 (0.177 mg m^{-2} Hz^{-1} for 5-MHz crystals); and n is the overtone number. Strictly speaking, the
209 Sauerbrey equation is valid for ultrathin rigid films whose frequency and dissipation changes
210 only depend on the mass of the film, especially for adsorbed polymers. A thin film can be
211 considered to be fully elastic and rigid when $\Delta D \leq 1 \cdot 10^{-6}$ and no clear spreading of the

overtones in the $\Delta f_n/n$ and ΔD_n graphs can be detected. Under such conditions, the Sauerbrey equation is valid for estimating the mass changes on the sensor surface.

A complete description of the kinetic modeling approach is described in Appendix 1 of the Supplementary Materials (SM).

Characterization of CNC surfaces coated with xylan fractions

AFM: Topographical images of silicon wafers were recorded by atomic force microscopy (AFM) using an Innova AFM (Bruker). The images were collected in tapping mode under ambient air conditions (temperature and relative humidity) using a monolithic silicon tip (TESPA, Bruker) with a spring constant of 42 N m^{-1} and a nominal frequency of 320 kHz. Image processing was performed using WSxM 5.0 software.

Molecular dynamics (MD) simulations

The models considered in this study consisted of three molecular species: a cellulose microfibril, xylan chains and water molecules. The cellulose microfibril model contained 18 chains of cellulose (Kubicki et al., 2018) in the Iβ organization and exposed the (110), (1-10) and (100) surfaces (Mazeau, 2011). The two primitive cell chains of the Iβ allomorph (Nishiyama, Langan, & Chanzy, 2002) were first duplicated through space, and a P_1 periodic super-crystal was redefined, which consisted of 6x6 cellulose chains. Each individual chain consisted of six anhydroglucose units and was covalently bonded to its own periodic image, mimicking a chain of infinite length. The supercell was then equilibrated using NPT-MD (constant number of particles, pressure and temperature) at 300 °K and 1 atm. The **a** and **b** parameters of the periodic cell were then increased to 50 Å and the excess cellulose chains were removed to retain only 18 chains. The **c** parameter was maintained at its equilibrium value of 31.4 Å. A charged sulfate group (SO_3^-) was added on an O-6 oxygen atom of the (1-

237 10) surface to model a cellulose crystal prepared by sulfuric acid, and a Na^+ cation was also
238 inserted in the simulation box to ensure the neutrality of the system. The model is infinitely
239 long in the longitudinal direction but finite in the perpendicular direction. This model was
240 then hydrated using the simple three-point-charges water model (Berendsen, Postma, Van
241 Gunsteren, & Hermans, 1981) and equilibrated by 50 ns of NVT-MD (constant number of
242 particles, volume and temperature) at 400 °K. This equilibration resulted in a conformational
243 change of the hydroxyl and hydroxymethyl groups exposed to the water environment, the
244 hydroxyl groups created hydrogen bonds with the water molecules, and the surface
245 hydroxymethyl groups rotated from the *tg* orientation to a mixture of the *gg* and *gt*
246 orientations. The water molecules were then removed to generate the initial models of the
247 cellulose-xylan complexes.
248 Xylan chains consisted exclusively of six skeletal anhydroxylose units. They are either non-
249 substituted or per-acetylated. In the latter case, all of the units were O-acetylated at the O-2
250 and O-3 oxygen atoms. Two helical conformations, 2_1 and 3_2, of the xylan skeleton were
251 considered. Their coordinates were extracted from a previous study (Mazeau, Moine, Krausz,
252 & Gloaguen, 2005). For the two helical conformations of the per-acetylated xylan chain, the
253 initial orientation of the acetyl groups corresponded to the lowest energy extracted from a
254 Monte-Carlo sampling of 1000 conformations on an isolated chain with a rigid backbone
255 (SM, Appendix 2).
256 The xylan chains were inserted in the simulation box around the cellulose microfibril. They
257 were aligned with the microfibril, either parallel or antiparallel at random. Similar to the
258 cellulose chains, the xylan chains were linked to their periodic images by covalent bonds in
259 order to mimic infinitely long chains. The two acetylated models, XylAc, consisted of 20
260 chains of fully acetylated xylan chains (total mass: 25920 g mol^{-1}), whereas the two non-
261 acetylated models, XyldAc, consisted of 33 chains of non-substituted xylan chains (26136 g

262 mol^{-1}). Water molecules where then added in the remaining empty spaces of the simulation
263 boxes.
264 The models were then subjected to energy minimizations followed by MD simulations. The
265 first energy minimization was performed while maintaining the cellulose and xylan chains
266 frozen; only the positions of the water molecules were refined at this step. All the atoms were
267 free to move in the second minimization step. The MD simulations were performed in the
268 NVT ensemble at 400 °K (50 ns), and then at 298 °K (10 ns). The coordinates of the cellulose
269 microfibril were frozen during the MDs. MD simulations were long enough to reach
270 equilibration when the energy, location and conformation of the xylan chains were stable. The
271 last ns of the room-temperature trajectories were used for analysis.
272
273 *Computational details*
274 Material Studio modeling software (v5.5) was used (Accelrys, Inc., San Diego, CA, USA).
275 Energy calculations were performed using the Universal Force Field (Rappe, Casewit,
276 Colwell, Goddard, & Skiff, 1992). This all-atoms force field was applied in our previous
277 study of cellulose-xylan complexes (Mazeau & Charlier, 2012) and it was also used for the
278 development of a coarse grain force field (Li, Perre, Frank, & Mazeau, 2015). The charge
279 equilibration method was used to calculate partial charges for each atom (Rappe & Goddard,
280 1991). The long-range interactions were calculated using the particle-mesh Ewald summation
281 method (Darden, York, & Pedersen, 1993) with a cut-off distance of 9 Å.
282 Energy minimization was performed by the steepest descent method and then by the
283 conjugated gradient method. The convergence criterion was a root-mean-square (rms) force of
284 less than 0.1 $kcal.mol^{-1}.Å^{-1}$. The integration of Newton's laws of motion in the MD
285 simulations was performed using the standard Verlet algorithm (Verlet, 1967) with a time step

of 0.001 ps. The total external pressure was maintained at 1 atm (Berendsen et al., 1981) and a Hoover algorithm (Evans & Holian, 1985) was used to keep the cell temperature constant.

RESULTS

XylAc and XyldAc fractions extraction and characterization

Investigation of the hemicellulose function in the plant cell wall requires careful extraction in order to provide a structure representative of those naturally occurring *in planta*. However, hemicellulose is classically extracted with alkali, leading to the hydrolysis of the acetyl ester groups. In a previous study, a non-aqueous polar aprotic solvent, namely DMSO doped with LiCl, was used to efficiently extract acetyl-esterified hemicelluloses (Assor et al., 2013; Ray et al., 2014). Applying this extraction procedure to apple pomace after partial removal of pectin followed by anion exchange chromatography allowed the recovery of a xylan-enriched fraction (XylAc). Fig. S1 reviews the overall extraction process. The extract was composed in decreasing order of weight proportion as follows: xylose, uronic acid, arabinose and acetyl esters, as well as low amounts of glucose, galactose and mannose and traces of fucose (Table 1). Mild alkali treatment of the fraction succeeded in removing acetyl esters with limited changes in the sugar composition (Table 1). The extract was thus mainly enriched in arabinoxylan (GAX), whose composition was close to that reported for Gala GAX (Ray et al., 2014) except for the presence of glucuronic acid, though comparatively richer in acetyl esters (7.2% vs. 3.8% in Gala). The presence of low amounts of glucose, mannose, galactose and fucose indicates the likely contamination of the AX by some galactoglucomannan and xyloglucan, whereas the galacturonic acid and rhamnose content suggests the presence of remaining pectin. Assuming that all acetyl esters were related to the xylan and were linked to the xylose residue, there would be one acetyl group for approximately two xylose residues, in

311 agreement with the average distribution of acetyl ester in plant xylan (Busse-Wicher et al.,
312 2014; Chong et al., 2014; Grantham et al., 2017). Glucuronic acid and arabinose are present in
313 the proportion of one uronic acid for approximately three xyloses, instead of one to six
314 xyloses in the *Arabidopsis* primary wall and one arabinose for approximately 3.4 xylose
315 residues, which could account in part for the pentose unit linked to glucuronic acid in the
316 *Arabidopsis* primary wall xylan (Mortimer et al., 2015).

317

318 Table 1. Chemical composition of the acetylated (XylAc) and deacetylated (XyldAc) xylan
319 fractions. Total sugars (TS) and the acetyl group contents are expressed in wt% and
320 monosaccharide content is expressed in mol%.

	Acetyl	*TS*	*Glc*	*Gal*	*Man*	*Xyl*	*Ara*	*Fuc*	*Rha*	*GalA*	*GlcA*
	(wt%)						*(mol%)*				
XylAc	7.2	78.3	5.4	5.1	2.3	51.9	16.5	0.2	1.0	16.5	1.0
XyldAc	0	77.6	4.9	5.0	2.7	53.6	16.9	0.3	1.0	14.8	0.9

321

322 *Adsorption of XylAc and XyldAc fractions on the cellulose model surface*

323 Spin-coated CNCs prepared from cotton linters were used as a model surface. They displayed
324 the expected rod-like morphology with dimensions of approximately 175 nm in length, 15 nm
325 in width and 7 nm in thickness, consistent with previous reports (Cherhal, Cousin, & Capron,
326 2015). The ability of XylAc and XyldAc-enriched fractions to adsorb on the CNC surface was
327 evaluated and compared by QCM-D. This technique relies on the properties of piezoelectric
328 quartz sensors submitted to an electric field that induces mechanical shear wave of the crystal.
329 Adsorption of any material on the quartz surface induces a shift in the frequency resonance
330 (Δf_n), allowing real-time monitoring of polymer adsorption on the quartz surface. Thanks to
331 its very high sensitivity, the technique has been successfully used to monitor a wide range of

adsorption processes. The second piece of information that can be obtained from the QCM-D analysis is the dissipation factor ΔD. This value provides an indication of the mechanical (viscoelastic) behavior of the layer adsorbed on the quartz since it reflects how the layer will dissipate the energy of the oscillation waves of the quartz sensor. QCM-D has already been used for the investigation of adsorption of xylan and xylan derivatives (Dammak et al., 2013; Kohnke et al., 2011; Sang Hoon Lee, Lee, & Youn, 2014; S. H. Lee, Lee, & Youn, 2015). Prior to QCM-D analysis, the xylan fractions were adsorbed on the CNC surfaces and the morphology was analyzed by atomic force microscopy (Fig. S2). In all the cases, the CNCs were easily visible and the complexes showed no clear differences with the initial CNC surface. This indicates that xylan is adsorbed as an individual polymer chain or, at most, as very small aggregates undetectable by AFM. In the following section, we report the frequency variations for different hemicellulose fractions, followed by an investigation of the dissipation patterns.

Frequency variation during XylAc and XyldAc adsorption and kinetic modeling of the adsorption behaviors

Prior to injection, the CNC surfaces were stabilized with water and the xylan fractions were injected at different concentrations ranging from 0.3 $\mu g\,mL^{-1}$ up to 20 $\mu g\,mL^{-1}$ to explore a large panel of ratios between polymers and adsorption sites. For the two fractions, acetylated and deacetylated, the decrease of frequencies observed, regardless of the concentration injected, indicated adsorption of xylan fractions on the cellulose surface. For each xylan concentration, adsorption was repeated at least three times to assess the reproducibility, and a typical frequency variation against time is reported in Fig. 1. Adsorption was irreversible since the rinsing steps applied after adsorption (indicated by arrows on Fig. 1) did not change the frequency values.

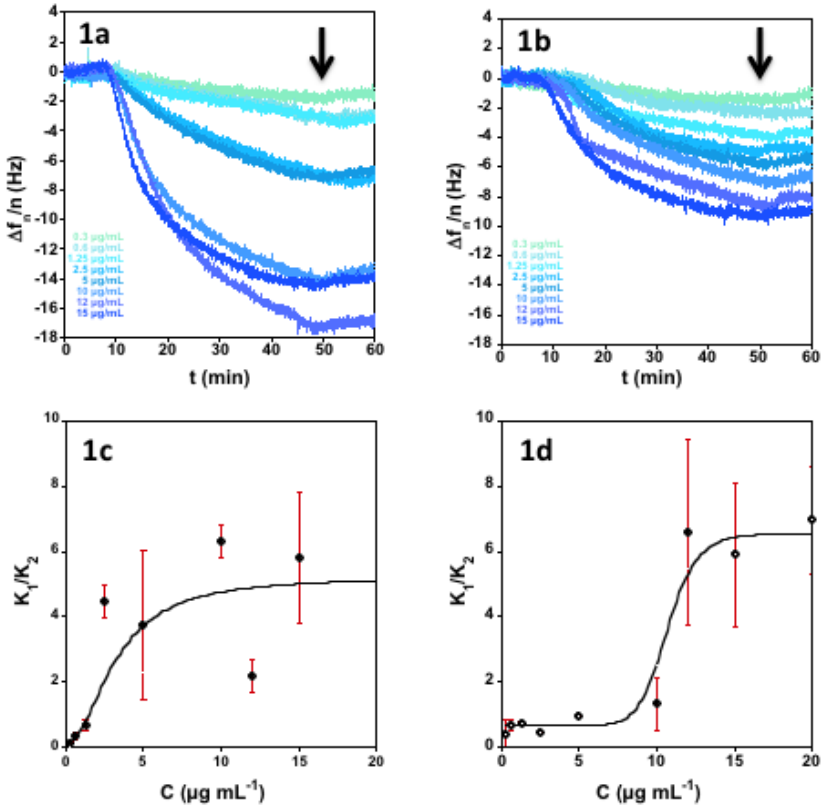

356

357 **Fig. 1**. Frequency (Δf_n) (3rd overtone) for the adsorption of XylAc (1a) and XyldAc (1b)
358 fractions and evolution of the k_1/k_2 ratio as a function of the XylAc (1c) or XyldAc (1d)
359 concentration (solid lines are visual guides). Arrows indicate the beginning of the rinsing step
360 with water.

361

362 For the XylAc and XyldAc fractions, different maximal frequency values were obtained for
363 all concentrations studied, indicating that the final amount of xylan adsorbed depended on the
364 sample concentration applied, as previously reported for the xyloglucan adsorption on CNC
365 surfaces (Villares et al., 2017; Villares et al., 2015). Frequency variations were in the same
366 range (tens of Hz) for both xylan fractions, suggesting that the amounts adsorbed are similar,
367 contrary to Kabel *et al* results that reported a higher adsorption of the deacetylated fraction.
368 (Kabel, van den Borne, Vincken, Voragen, & Schols, 2007). This finding can be assigned to

a lower steric hindrance due to the removal of acetyl groups to increase the self-associative capacity of xylans, as reported earlier by Linder (Bosmans et al., 2014; Linder, Bergman, Bodin, & Gatenholm, 2003). Since both the XylAc and XyldAc fractions did not desorb from the surface during the time scale of the experiment, the maximal frequencies cannot be attributed to a dynamic equilibrium between adsorption and desorption of the polymer. Moreover, the continuous flow of XylAc and XyldAc on the surface guaranteed that the maximum coverage possible for each condition was reached. Thus, this pattern suggests that the final amount of polymer adsorbed depended on the competition between adsorption, packing optimization and potential rearrangement, suggesting that the adsorption process is therefore not the result of thermodynamic equilibrium but, instead, is kinetically-driven.

We previously described such behavior by using a kinetic model that comprises two steps: the first one describes the adsorption of hemicellulose onto an uncovered surface associated with the rearrangement of the chains to cover the surface, and the second corresponds to adsorption on a covered surface on which the polymer must diffuse through a pre-adsorbed hemicellulose layer (Villares et al., 2017). This kinetic model was used to determine k_1 and k_2 for the XylAc and XyldAc fractions that are the kinetic constant for the first and second adsorption steps, respectively. The detailed mathematical expressions of the kinetic model and typical fits obtained are given in the Supplementary Material (SM, Appendix 1). The experimental fractional coverage was calculated to obtain values of the kinetic constants k_1 and k_2, and there was a good fit between experimental and calculated values (Fig. S3). The evolution of the ratio k_1/k_2 against the XylAc and XyldAc fraction concentration is plotted in Fig. 1c and d, respectively. The fractions display different patterns with two domains of concentrations.

At low concentration, the k_1/k_2 ratio is lower or close to one indicating that the kinetic adsorption and lateral rearrangement occur at a similar time scale, leading to large amounts of

extended xylan conformation or trains. At higher concentrations, adsorption occurs through diffusion on the pre-adsorbed layer, and the crowding of the surface limits diffusion and rearrangement mechanisms. Thus, the k_1/k_2 ratio increases since the adsorption process on a bare surface (k_1) dominates, while (k_2) decreases dramatically. The increase of the k_1/k_2 ratio associated with a higher amount of polymer adsorbed can be interpreted either by a denser packing of the molecules when the concentration increases or by limited rearrangement possibilities. A clear difference can be seen between acetylated and deacetylated xylan. In the case of the XylAc fraction, the k_1/k_2 ratio increases very rapidly, suggesting that even at low concentrations, the acetylated sample is able to efficiently cover the surface and the possibility of rearrangement seems to be strongly limited, suggesting efficient interactions between XylAc and the cellulose surface. In the case of XyldAc, a transition between the two regimes (i.e., the concentration at which the k_1/k_2 ratio increases) is clearly seen at around 5-10 μg mL^{-1}. This suggests that chain rearrangements can occur at low surface concentrations, whereas surface crowding may limit conformation modification at higher concentrations. Nevertheless, the presence of acetyl groups changes the adsorption behavior of the xylan chains and the acetylated fraction seems to have a greater ability to cover the surface than the deacetylated one.

Comparison of the viscoelasticity behaviors of adsorbed layers

To correlate the evolution in dissipation with changes in frequency, the ΔD was plotted as a function of Δf (hereafter referred to as ΔD *vs.* Δf plots) to eliminate time as an explicit parameter (Fig. 2). The raw dissipation data for both fractions at different concentrations are illustrated in Figs. 2a and 2b. The ΔD *vs.* Δf plots revealed different slopes of the curves that are related to the overall viscoelasticity of the layer. A rigid layer will behave similarly to the quartz dissipation and the ΔD will present low values per mass addition and, accordingly, the ΔD *vs.* Δf slope will be low. In the case of a more viscoelastic layer, the ΔD *vs.* Δf slope will

display higher values. As shown in Figs. 2c and 2d, the two xylan fractions display strikingly different behaviors. The slope obtained for XylAc is constant (0.03 10^{-6} Hz^{-1}) regardless of the concentration studied, indicating that irrespective of concentration, the adsorbed acetylated xylan layer on cellulose shares a similar organization. Moreover, the very low value of the slope suggests that the adsorbed layer is rigid. This finding is consistent with the kinetic analysis that displays only one regime of adsorption in which the k_1 constant is dominant and which suggests that the XylAc layer is strongly adsorbed with limited diffusion and rearrangement processes. It should be emphasized that the slope value of the *ΔD vs. Δf* of XylAc is significantly lower compared to the values found in the literature. For example, Eeronen et al. (Eronen et al., 2011) reported a value of 0.25 10^{-6} Hz^{-1} for wheat arabinoxylans and of 0.1 10^{-6} Hz^{-1} for spruce galactoglucomanans, which are on the same order of magnitude as the value measured for the XyldAc but almost ten times higher than the value of 0.03 10^{-6} Hz^{-1} determined for the XylAc. This finding suggests that the mechanical properties of the XylAc layer are quite similar to those of the cellulose surface and can probably be attributed to flat and dense layers.

In contrast, the *ΔD vs. Δf* plot of XyldAc displays different slopes depending on the injection concentration, indicating a more complex behavior (Fig. 2d). The *ΔD vs. Δf* plot pattern evolved during the adsorption process, suggesting a change in layer organization during adsorption. At low concentrations (<5 μg mL^{-1}), the slope value is around 0.25-0.5 10^{-6} Hz^{-1}, whereas at higher concentrations, the value decreases to 0.1-0.15 10^{-6} Hz^{-1}. At low concentrations, the slope value is high, which indicates a high viscosity of the layer, and then starts to decrease to reach a stable value at a concentration of 5-10 μg mL^{-1}. This suggests the formation of a loose layer that becomes denser as the concentration increases.

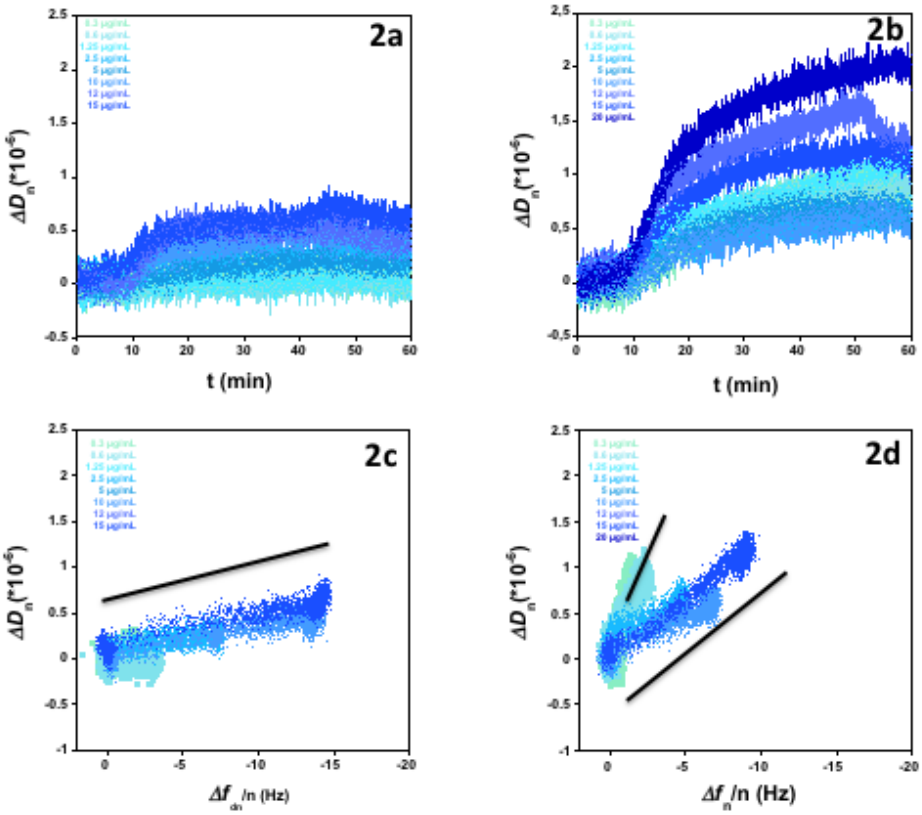

442

443 **Fig. 2**. Dissipation (ΔD) (3rd overtone) for the adsorption of XylAc (2a) and XyldAc (2b)
444 fractions for different concentrations as a function of time and corresponding ΔD *vs.* Δf plots
445 for XylAc (2c) and XyldAc (2d) (solid lines are visual guides).

446

447 *Adsorption of XylAc and XyldAc fractions on the cellulose model surface by MD*

448 Four models of the hydrated cellulose xylan complex that differed by the chemical structure
449 of their xylan chains and by their initial conformation were considered. The xylan chains were
450 either acetylated or non-acetylated (corresponding to deacetylated sample). Repeat unit is
451 shown in Fig S4. In addition, to account for the conformational polymorphism of xylan
452 (Chanzy, Dube, & Marchessault, 1979; Larsson, 2004; Teleman, Larsson, & Iversen, 2001),
453 the xylans differed by the initial helical conformation of their backbone: either two units per
454 helical turn when the xylan chains contained three turns of the 2_1 helix in their initial state, or

three units per helical turn when they contained two turns of the left-handed 3_2 helix (Figs. S5 and S6).

The four models were subjected to MD simulations at two temperatures. During the high temperature phase, the xylan chains explored the two helical conformations with rapid inter-conversions between the two forms. This is not surprising since the two conformations have similar energies and the energy barrier between them, estimated from the adiabatic potential energy surface of xylobiose (Mazeau, Moine, Krausz, & Gloaguen, 2005), is lower than 2 kcal mol^{-1}. In contrast, during the room-temperature phase, each xylan chain stabilized in its preferred conformation depending on its immediate environment and remained in that conformation up to the end of the trajectory. As a consequence, the models that differed by the initial conformation of the xylan chains converged into an identical structure of the complex. Fig. 3 provides representative snapshots of the XylAc and XyldAc models.

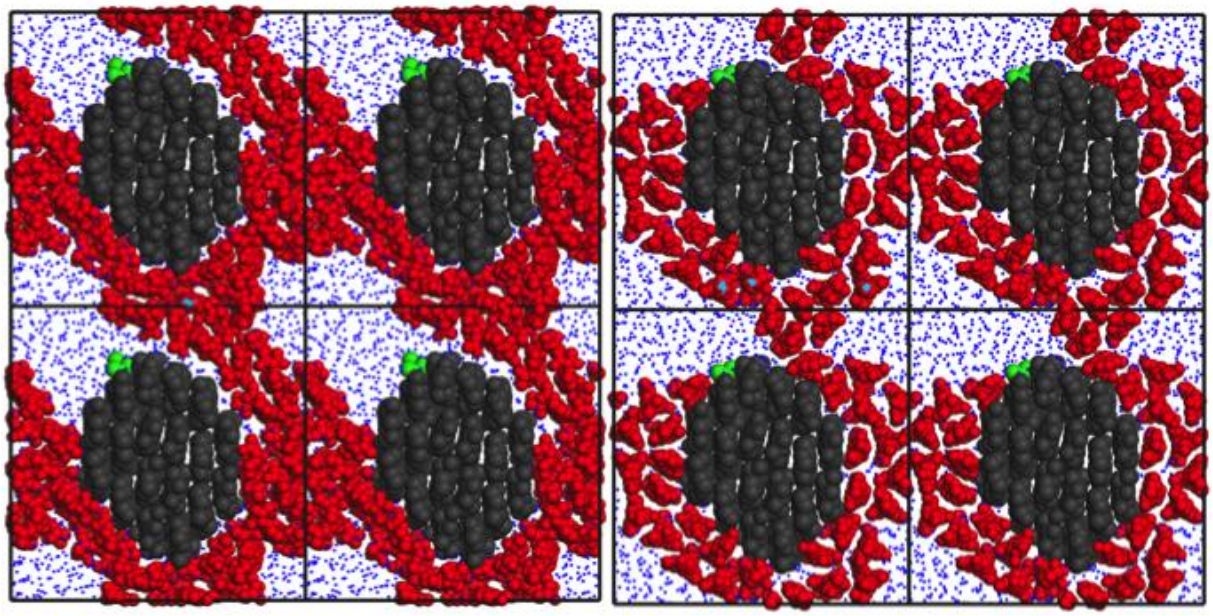

Fig. 3: Cross-sectional views of the models of the hydrated cellulose-xylan complexes. 2x2 basic cells are displayed. Hydrogen atoms are omitted for clarity. Cellulose is in gray. Sulfate group, in green, is located on a chain of the (1-10) surface of cellulose next to its top corner.

The xylan chains are in red and the water molecules in blue. Left: XylAc model; right XyldAc model.

Conformation of the xylan chains

Analysis of the helical conformations of the xylan chains in the equilibrated models is performed using the turn angle (T), which is defined by the sequence of atoms O-5''−C-5''−C-4−C-5 (Fig. S4). The turn angle describes the orientation of a given unit with respect to its second neighbor for those perfectly stereo-regular helices that were used to build the initial models T = -50° for the 2_1 helix and T=100° for the 3_2 helix.

Fig. 4 gives the distributions of the turn angle of the xylan chains in the equilibrated XylAc and XyldAc models. It shows the distributions of all the chains (denoted 'all'), together with that of the chains in close proximity to the cellulose, denoted '1st layer', and that of the chains far from the cellulose, denoted 'other layer'. For the purpose of comparison, the same calculations were performed for arged cellulose, and similar distributions were obtained in all cases (SM, Appendix 3 - Fig. S10 - S11-S12).

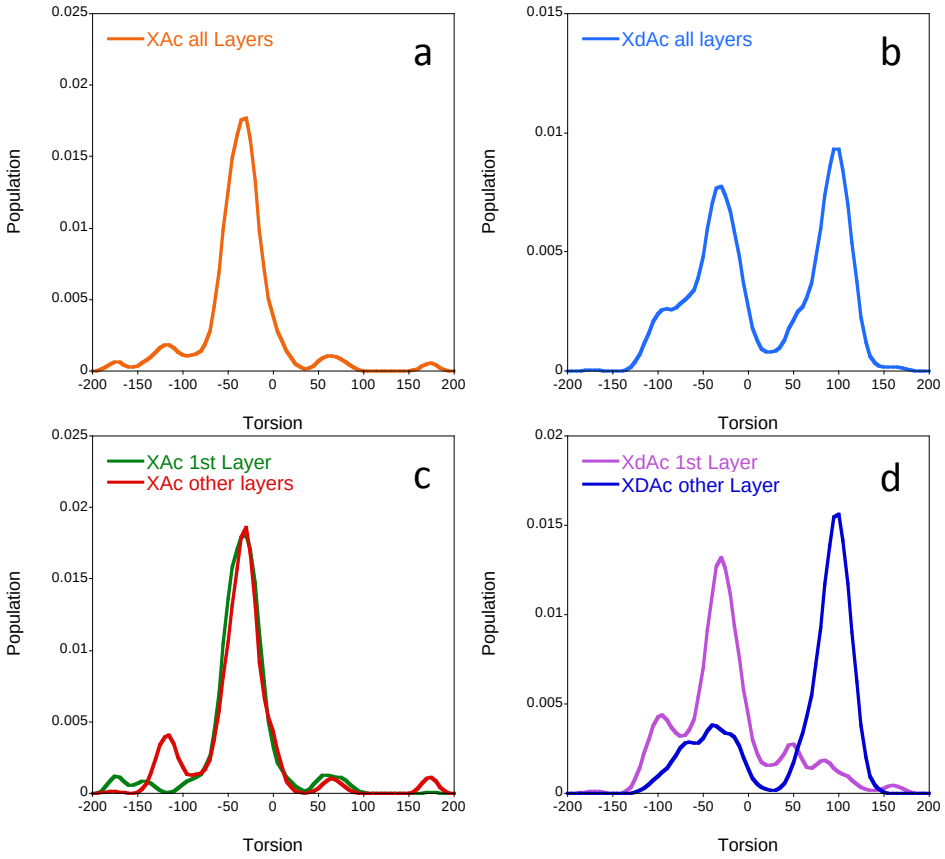

Fig. 4. Distribution of the turn angle in the XylAc (left) and XyldAc (right) simulated systemsGlobal distributions from all the xylan chains (4a and 4b); and distributions from the xylan chains interacting with cellulose (orange in 4c and light blue in 4d) and from the bulk xylan (red in 4c and dark blue in 4d).

For XylAc, the distribution is almost monomodal and centered at T=-35°. Considering the thermal motion and local conformational variability, this peak corresponds to helices with two residues per helical turn. The distribution of T also reveals other forms, non-canonical, less organized and of low occurrence, at T= -120°, 60° and 180°. Conformations of the xylan chains in the XyldAc model differ substantially. The bimodal distribution of the turn angle centered at T=-35° and +95° shows that the deacetylated xylan chains explore the two main 2_1 and 3_2 helical forms. It should be noted that most of the chains in direct interaction with

cellulose are mainly in the 2_1 conformation, whereas those far from the cellulose (in the bulk phase of xylan) are in the 3_2 conformation. Here again, a few chains explored alternative disorganized conformations, as suggested by the broad distribution of the turn angle.

Concentration profiles.

The concentration fluctuations of cellulose, xylan and water were determined along the 100 and 010 directions in both the immediate environment of the cellulose and in the bulk xylan (Fig. 5).

At the interface with cellulose, the acetyl groups do not affect the adsorption behavior of xylan. The concentration traces at 40 Å show a maximum for xylan and, concomitantly, a minimum for water, which is particularly visible on the profiles along the 100 direction. This reveals that xylan accumulates at the interface on the uncharged side of the cellulose crystal. The concentration profiles of xylan and water at the interface with cellulose are, however, dissymmetrical. At 10 Å in the plots, i.e., on the charged side of the cellulose, the xylan concentration is minimal, whereas that of water is maximal, which suggests that the charged sulfate group preferentially interacts with the surrounding water molecules rather than with xylans. Additional modeling was performed with a native (uncharged) cellulose crystal in order to estimate the exact effect of the charged sulfate group (see SM, Appendix 3, Figs. S11 and 12). The corresponding concentration traces with uncharged cellulose are in fact more symmetrical and show a high concentration of xylan and a low concentration of water at both interfaces. The charged sulfate group does not interact with the acetylated xylans but can occasionally form a hydrogen bond with a hydroxyl group of the deacetylated xylan. The charged sulfate group, along with its surrounding hydration shell, enhances the cellulose hydrophilicity, increases the porosity of the total system, and lowers the total cellulose surface covered by xylan.

In contrast, within the xylan phase, at around 0 or 50 Å in the concentration profiles, the acetyl groups have a strong influence on xylan organization. For XylAc, xylan concentration is similar to that of water, suggesting that the system is dense and weakly hydrated. This type of organization is obviously facilitated by the dominant 2_1 helical conformation of their backbones whose compact packing, similar to that of cellulose or chitosan, can be easily achieved. However, the multiple conformations explored by the acetyl groups disturb the perfection of the packing at the local level and create small cavities in which few water molecules can penetrate. For XyldAc, in contrast, xylan concentration is much lower than that of water, which suggests that the deacetylated xylan layer is loose and highly hydrated. The two free hydroxyl groups per repeat unit strongly interact with water molecules and the packing of the 3_2 helices promotes uninterrupted columns of water that appear in between the deacetylated xylan chains.

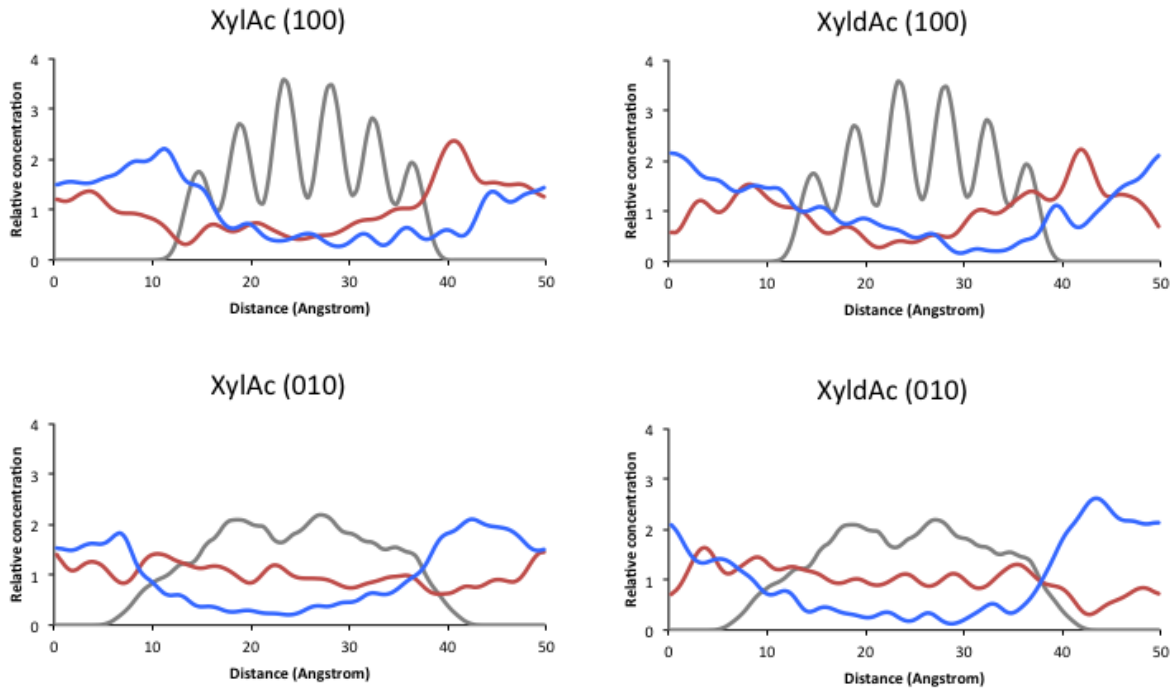

Fig. 5: Concentration profiles of cellulose, xylan and water along directions perpendicular to the exposed crystallographic planes of the cellulose. In gray: cellulose; in red: xylan; in blue: water.

Our models are consistent with experimental data from X-ray diffraction and solid-state NMR. The crystal structure of xylan diacetate is anhydrous and made of two-fold helices (Gabbay, Sundararajan, & Marchessault, 1972), whereas that of deacetylated xylan contains between one to three water molecules per xylosyl unit and the chains are in the left-handed three-fold helix (Nieduszynski & Marchessault, 1971; Nieduszynski & Marchessault, 1972). These deacetylated xylan chains also explore the three-fold conformation in a water solution but change their conformation to the two-fold one when interacting with cellulose (Larsson, Hult, Wickholm, Pettersson, & Iversen, 1999). It should be noted that such conformational adaptation is limited to those xylan chains in direct contact with the cellulose surface (Falcoz-Vigne et al., 2017).

In a modeling study, the two limiting cases were studied where xylan chains are either per-acetylated or deacetylated, whereas Busse-Wicher et al. modeled the adsorption of a partly-acetylated xylan chain in which the distribution of the acetyl groups is stereoregular, i.e., where every other xylose residue is acetylated (Busse-Wicher et al., 2014). Comparing the two studies makes it possible to determine the effects of the degree of acetylation in the xylan chain on its interaction with cellulose. The degree of acetylation does not affect the conformation of xylan in direct contact with cellulose, adopting the two residues per helical turn conformation. Acetylation also does not affect the adsorption features of xylan on the hydrophobic surface of cellulose. Instead, it stacks on this surface by its aliphatic C-H groups. The interaction on this particular cellulose surface is dominated by the Van der Waals forces (Martinez-Abad et al, 2017; Mazeau & Charlier, 2012). In contrast, the degree of acetylation affects the adsorption features of xylan on the hydrophilic surfaces of cellulose. The per-acetylated xylan adsorbs flat to maximize the number of Van der Waals contacts. This organization is obviously promoted by the amphiphilicity of the cellulose surfaces (Mazeau, 2011). On the contrary, the deacetylated xylan adsorbs in a tilted conformation to establish

564 hydrogen bonds between its hydroxyl groups and the hydroxyl groups protruding from the
565 cellulose surface. The regularly and alternately substituted xylan considered by Busse-Wicher
566 et al., which forms hydrogen bonds with cellulose, thus follows the adsorption of the non-
567 substituted xylan (Busse-Wicher et al., 2014). This similarity is understandable considering
568 that a xylan polymer in the 2_1 helical conformation in which only one residue out of two is
569 substituted has only one acetylated side. This is the non-substituted side, consisting only of
570 hydroxyl groups, that preferentially interacts with cellulose in the same way as a deacetylated
571 xylan.

572

573 **DISCUSSION**

574 Xylan presents a broad structural variability and is a major hemicellulose in plant biomass,
575 essentially encountered in secondary cell walls (Brummell & Schröder, 2009; Scheller &
576 Ulvskov, 2010). It is, however, a minor component of primary cell walls and particularly
577 those of fleshy fruit (Brummell & Schröder, 2009) such as apple where it occurs as
578 glucuronoarabinoxylan (GAX) (Ray et al., 2014). The proportions of uronic acids, arabinose
579 and acetyl ester substitutions determined for the apple pomace xylan fractions are similar to
580 those reported for Gala apple (Ray et al., 2014). Considering that apple pomace is not
581 lignified, it is therefore a convenient biological source for native xylan with a preserved
582 substitution pattern that can be used as a model polymer for *in vitro* investigation.

583 QCM-D experiments complemented by molecular modeling provide an atomistic-scale view
584 of the effect of the acetyl groups attached to xylan on their adsorption on cellulose.

585 Adsorption of xylan fractions followed by QCM-D demonstrated that the acetylated and
586 deacetylated fractions adsorption processes are both kinetically-driven but display different
587 behaviors. XylAc has an almost homogenous adsorption pattern for all concentrations (k_1

588 dominated), which suggests limited rearrangement after adsorption, whereas XyldAc displays
589 two clear concentration domains of adsorption (k_1/k_2 increased between 5 and 10 g L^{-1}). These
590 behaviors are also supported by the pattern of the *ΔD vs. Δf* representation. The *ΔD vs. Δf* plot
591 for XylAc displays a single slope, whereas that for XyldAc shows two slopes between 2.5 and
592 10 mg L^{-1} of xylan injected. The slope change corresponds to the increase of the k_1/k_2 ratio
593 observed in the kinetic modeling analysis. For the higher slope (low concentration), k_1/k_2 is
594 close to one and increase when the slope become lower. The models revealed that adsorption
595 of XylAc is straightforward since the acetylated xylan does not need to modify its solution
596 conformation (two-fold helices). In contrast, adsorption of the very first molecules of XyldAc
597 requires a conformational change to adopt a form complementary to that of cellulose (from
598 three-fold to two-fold), whereas the additional molecules adsorb without conformation change
599 (three-fold).

600 Additionally, the XylAc *ΔD vs. Δf* slope displays a very low and homogeneous value (0.03 10^{-6}
601 Hz^{-1}) compared to XyldAc fraction values that are higher and variable according to the
602 concentration injected (from 0.5 to 0.1 10^{-6} Hz^{-1}). This suggests the formation of a stiff and
603 densely-packed XylAc layer, whereas the XyldAc fraction forms a more viscous layer that
604 can be densified with increasing XyldAc concentration. In agreement with the experimental
605 observations, the models also show that the acetyl groups affect the compactness and
606 hydration of the xylan layer surrounding the cellulose. It is compact and weakly hydrated for
607 acetylated xylan, but loose and highly hydrated for deacetylated xylan. Considering that water
608 plasticizes hemicellulose, complexes made with XylAc would be rigid, as revealed by the low
609 gradient of the *ΔD vs. Δf* plot, whereas those made with XyldAc would be softer, showing a
610 more viscous character, as suggested by the larger slopes of the *ΔD vs. Δf* plot. The adsorption
611 process of the acetylated and deacetylated xylans on cellulose can be illustrated with the
612 schematics shown in Fig. 6.

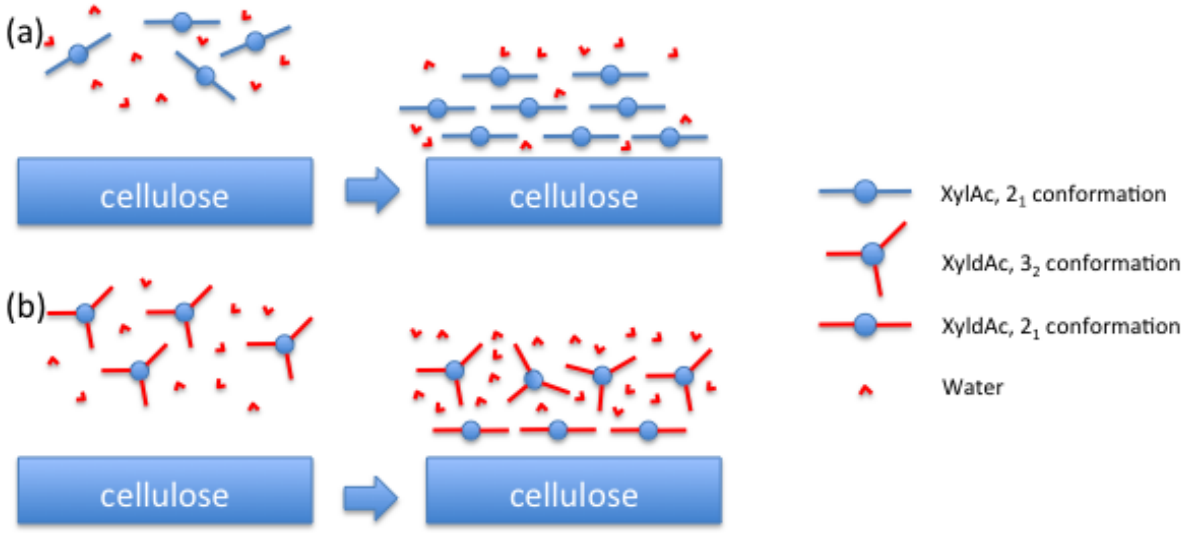

Fig. 6. Schematic representation of the adsorption process of XylAc (a) and XyldAc (b) on cellulose. Adsorption of XylAc results in the formation of a rigid (almost) anhydrous layer, whereas XyldAc forms a water-swollen soft layer.

Our findings indicated that the presence of acetyl esters influences the supramolecular organization of the xylan and its interaction with the cellulose surface. Deacetylated and acetylated xylans display different organization suggesting that the remaining substituent groups are not enough to keep the xylan interaction with cellulose surface unchanged. Indeed, in *Arabidopsis* mutants with decreased acetyl ester, compensation is provided by an increase in glucuronic (Grantham et al., 2017). In our case, the removal of all acetyl groups cannot be compensated by the other substituents.

The functional role of xylan in fleshy fruit remains unknown. In tomato, the trace amount of xylan was localized in cell walls lining intercellular space (Ordaz-Ortiz, Marcus, & Knox, 2009) and particularly in the skin and inner epidermal cells of the pericarp (Takizawa et al., 2014). In biomass, it is found in the secondary wall (Carafa, Duckett, Knox, & Ligrone, 2005) and directly or indirectly contributes to the mechanical properties of the stems (Li et al., 2015; Dammstrom, Salmen, & Gatenholm, 2009). The biological and technological roles of acetyl

groups are still unclear but it has been hypothesized that they limit the saccharification and fermentation of biomass (Pawar et al., 2017). Besides the steric hindrance induced by acetyl groups to access a xylanase catalytic site, the formation of a poorly hydrated and stiff layer interacting with cellulose, as suggested by our study, can also be an explanation for the limited xylanase accessibility and mechanical properties of plant cell walls.

CONCLUSION

Combined QCM-D and MD approaches were used to illustrate the impact of acetyl decoration on the interaction between xylan and cellulose. Both *in vitro* and *in silico* results showed that acetyl groups attached to the xylan chains significantly influence the conformational behavior of xylan and the supramolecular organization of the cellulose-xylan complex. Acetylated fractions adsorbed on cellulose form a dense and poorly hydrated layer, whereas the deacetylated fraction forms a more hydrated layer. It should be noted that the acetylated fraction has the two residue per turn conformation for all the adsorbed chains, whereas this conformation is limited to the xylan chains in direct contact with the cellulose surface for the deacetylated fraction. Our study therefore supports the assumption that the acetylation pattern promotes different organizations and hydrations of xylan cellulose complexes that can modulate the interaction strength and rheological properties of the cell wall xylan-cellulose supramolecular complexes. Our future studies will focus on the evaluation of the influence of the presence of the acetyl groups on the properties as well as the use of the modulation of acetylation patterns to implement xylan/CNC-based composites.

ASSOCIATED CONTENT

Supporting Information

DOI:

AUTHOR INFORMATION

Corresponding Author

*Email: Bernard.cathala@inra.fr

INRA, UR1268 Biopolymères Interactions Assemblages, Rue de la Géraudière, BP 71627, 44316 Nantes, France.

Tel. 00 33 (0)2 40 67 50 68

ACKNOWLEDGEMENTS

We gratefully acknowledge the computational resources at the Centre d'Expérimentation et de Calcul Intensif, CECIC, ICMG, Grenoble. Part of this work was performed on the BIBS instrumental platform (http://www.bibs.inra.fr/ bibs_eng/, UR1268 BIA, IBiSA, Phenome-Emphasis-FR ANR-11-INBS- 0012).

REFERENCES

Assor, C., Quemener, B., Vigouroux, J., & Lahaye, M. (2013). Fractionation and structural characterization of LiCl-DMSO soluble hemicelluloses from tomato. *Carbohydrate Polymers*, 94 (1), 46-55.

Benselfelt, T., Cranston, E. D., Ondaral, S., Johansson, E., Brumer, H., Rutland, M. W., & Wågberg, L. (2016). Adsorption of Xyloglucan onto Cellulose Surfaces of Different Morphologies: An Entropy-Driven Process. *Biomacromolecules*, 17(9), 2801-2811.

Berendsen, H. J. C., Postma, J. P. M., Van Gunsteren, W. F., & Hermans, J. (1981). Interaction models for water in relation to protein hydration. *Jerusalem Symp. Quantum Chem. Biochem.*, 14, 331-342.

Blumenkrantz, N., & Asboe-Hansen, G. (1973). New method for quantitaive determination of uronic acids. *Analytical biochemistry*, 54, 484-489.

Bosmans, T. J., Stépán, A. M., Toriz, G., Renneckar, S., Karabulut, E., Wågberg, L., & Gatenholm, P. (2014). Assembly of Debranched Xylan from Solution and on Nanocellulosic Surfaces. *Biomacromolecules*, 15(3), 924-930.

Brummell, D. A., & Schröder, R. (2009). Xylan metabolism in primary cell walls. *New Zealand Journal of Forestry Science*, 30, 125-143.

Busse-Wicher, M., Gomes, T. C. F., Tryfona, T., Nikolovski, N., Stott, K., Grantham, N. J., . . . Dupree, P. (2014). The pattern of xylan acetylation suggests xylan may interact with cellulose microfibrils as a twofold helical screw in the secondary plant cell wall of Arabidopsis thaliana. *Plant Journal*, 79(3), 492-506.

Carafa, A., Duckett, J. G., Knox, J. P., & Ligrone, R. (2005). Distribution of cell-wall xylans in bryophytes and tracheophytes: new insights into basal interrelationships of land plants. *New Phytol*, 168(1), 231-240.

690 Chanzy, H., Dube, M., & Marchessault, R. H. (1979). Structural polymorphism of (1-4)-beta-
691 D-xylan. *Polymer*, 20(8), 1037-1039.
692 Cherhal, F., Cousin, F., & Capron, I. (2015). Influence of Charge Density and Ionic Strength
693 on the Aggregation Process of Cellulose Nanocrystals in Aqueous Suspension, as
694 Revealed by Small-Angle Neutron Scattering. *Langmuir*, 31(20), 5596-5602.
695 Chong, S.-L., Virkki, L., Maaheimo, H., Juvonen, M., Derba-Maceluch, M., Koutaniemi, S., .
696 . . Tenkanen, M. (2014). O-Acetylation of glucuronoxylan in Arabidopsis thaliana
697 wild type and its change in xylan biosynthesis mutants. *Glycobiology*, 24(6), 494-506.
698 Dammak, A., Moreau, C., Beury, N., Schwikal, K., winter, H., Bonnin, E., . . . Cathala, B.
699 (2013). Elaboration of multilayered thin films based on cellulose nanocrystals and
700 cationic xylans: application to xylanase activity detection. *Holzforschung*, 67(5).
701 Dammstrom, S., Salmen, L., & Gatenholm, P. (2009). On the interactions between cellulose
702 and xylan, a biomimetic simulation of the hardwood cell wall. *Bioresources*, 4(1), 3-
703 14.
704 Darden, T., York, D., & Pedersen, L. (1993). Particle mesh Ewald: an N·log(N) method for
705 Ewald sums in large systems. *J. Chem. Phys.*, 98, 10089-10092.
706 Dheilly, E., Le Gall, S., Guillou, M. C., Renou, J. P., Bonnin, E., Orsel, M., & Lahaye, M.
707 (2016). Cell wall dynamics during apple development and storage involves
708 hemicellulose modifications and related expressed genes. *Bmc Plant Biology*, 16.
709 Eronen, P., Osterberg, M., Heikkinen, S., Tenkanen, M., & Laine, J. (2011). Interactions of
710 structurally different hemicelluloses with nanofibrillar cellulose. *Carbohydrate*
711 *Polymers*, 86(3), 1281-1290.
712 Escudero, V., Jorda, L., Sopena-Torres, S., Melida, H., Miedes, E., Munoz-Barrios, A., . . .
713 Molina, A. (2017). Alteration of cell wall xylan acetylation triggers defense responses

714 that counterbalance the immune deficiencies of plants impaired in the beta-subunit of
715 the heterotrimeric G-protein. *Plant J*, 92(3), 386-399.
716 Evans, D. J., & Holian, B. L. (1985). The Nose-Hoover thermostat. *J. Chem. Phys.*, 83(8),
717 4069-4074.
718 Falcoz-Vigne, L., Ogawa, Y., Molina-Boisseau, S., Nishiyama, Y., Meyer, V., Petit-Conil,
719 M., Mazeau, K. Heux, L. (2017). Quantification of a tightly adsorbed monolayer of
720 xylan on cellulose surface. *Cellulose (Dordrecht, Neth.)*, 24(9), 3725-3739.
721 Filisetti-Cozzi, T., & Carpita, N. (1991). Measurement of uronic acids without interference
722 from neutral sugars. *Anal. Biochem.* 197(1), 1, 157-162.
723 Gabbay, S. M., Sundararajan, P. R., & Marchessault, R. H. (1972). X-ray and stereochemical
724 studies on xylan diacetate. *Biopolymers*, 11(1), 79-94.
725 Gatenholm, P., & Tenkanen, M. (2004). *Hemicelluloses: Sciences and Technology*.
726 Washington C, USA: American Chemical Society.
727 Grantham, N. J., Wurman-Rodrich, J., Terrett, O. M., Lyczakowski, J. J., Stott, K., Iuga, D., .
728 . . Dupree, P. (2017). An even pattern of xylan substitution is critical for interaction
729 with cellulose in plant cell walls. *Nature Plants*, 3(11), 859-865.
730 Kabel, M. A., van den Borne, H., Vincken, J.-P., Voragen, A. G. J., & Schols, H. A. (2007).
731 Structural differences of xylans affect their interaction with cellulose. *Carbohydrate*
732 *Polymers*, 69(1), 94-105.
733 Kittle, J. D., Qian, C., Edgar, E., Roman, M., & Esker, A. R. (2018). Adsorption of
734 Xyloglucan onto Thin Films of Cellulose Nanocrystals and Amorphous Cellulose:
735 Film Thickness Effects. *ACS Omega*, 3(10), 14004-14012.
736 Kohnke, T., Ostlund, A., & Brelid, H. (2011). Adsorption of Arabinoxylan on Cellulosic
737 Surfaces: Influence of Degree of Substitution and Substitution Pattern on Adsorption
738 Characteristics. *Biomacromolecules*, 12(7), 2633-2641.

739 Kubicki, J. D., Yang, H., Sawada, D., O'Neill, H., Oehme, D., & Cosgrove, D. (2018). The
740 Shape of Native Plant Cellulose Microfibrils. *Scientific reports,* 8(1), 13983-13983.
741 Kumar, M., Campbell, L., & Turner, S. (2016). Secondary cell walls: biosynthesis and
742 manipulation. *J Exp Bot,* 67(2), 515-531.
743 Larsson, P. T. (2004). *Interaction between cellulose I and hemicelluloses studied by spectral*
744 *fitting of CP/MAS C-13-NMR spectra*. In P. Gatenholm & M. Tenhanen (Eds.),
745 *Hemicelluloses: Science and Technology* (pp. 254-268)
746 Larsson, P. T., Hult, E. L., Wickholm, K., Pettersson, E., & Iversen, T. (1999). CP/MAS 13C-
747 NMR spectroscopy applied to structure and interaction studies on cellulose I. *Solid*
748 *State Nucl Magn Reson,* 15(1), 31-40.
749 Lee, S. H., Lee, H. L., & Youn, H. J. (2014). Adsorption and viscoelastic properties of
750 cationic xylan on cellulose film using QCM-D. *Cellulose,* 21(3), 1251-1260.
751 Lee, S. H., Lee, H. L., & Youn, H. J. (2015). Adsorption of Xylan onto Cellulose Fibers
752 Pretreated with Cationic Polyelectrolyte and Its Effect on Paper Properties.
753 *Bioresources,* 10(1), 851-865.
754 Levigne, S., Thomas, M., Ralet, M. C., Quemener, B., & Thibault, J. F. (2002). Determination
755 of the degrees of methylation and acetylation of pectins using a C18 column and
756 internal standards. *Food Hydrocolloids,* 16(6), 547-550.
757 Li, L., Perre, P., Frank, X., & Mazeau, K. (2015). A coarse-grain force-field for xylan and its
758 interaction with cellulose. *Carbohydr. Polym.,* 127, 438-450.
759 Linder, A., Bergman, R., Bodin, A., & Gatenholm, P. (2003). Mechanism of asembly of xylan
760 onto cellulose surfaces. *Langmuir,* 19, 5072-5077.
761 Martinez-Abad, A., Berglund, J., Toriz, G., Gatenholm, P., Henriksson, G., Lindstrom, M., . .
762 . Vilaplana, F. (2017). Regular Motifs in Xylan Modulate Molecular Flexibility and
763 Interactions with Cellulose Surfaces. *Plant Physiology,* 175(4), 1579-1592.

764 Mazeau, K. (2011). On the external morphology of native cellulose microfibrils. *Carbohydr.*
765 *Polym.*, 84(1), 524-532.
766 Mazeau, K., & Charlier, L. (2012). The molecular basis of the adsorption of xylans on
767 cellulose surface. *Cellulose,* 19(2), 337-349.
768 Mazeau, K., & Charlier, L. (2012). The molecular basis of the adsorption of xylans on
769 cellulose surface. *Cellulose (Dordrecht, Neth.),* 19(2), 337-349.
770 Mazeau, K., Moine, C., Krausz, P., & Gloaguen, V. (2005). Conformational analysis of xylan
771 chains. *Carbohydrate Research,* 340(18), 2752-2760.
772 Mazeau, K., Moine, C., Krausz, P., & Gloaguen, V. (2005). Conformational analysis of xylan
773 chains. *Carbohydrate research,* 340(18), 2752-2760.
774 Melton, L. D., Smith, B. G., Ibrahim, R., & Schröder, R. (2009). Mannans in primary and
775 secondary plant cell walls. *New Zealand J. Forestry Sci.*, 39, 153-160.
776 Mortimer, J. C., Faria-Blanc, N., Yu, X., Tryfona, T., Sorieul, M., Ng, Y. Z., . . . Dupree, P.
777 (2015). An unusual xylan in Arabidopsis primary cell walls is synthesised by GUX3,
778 IRX9L, IRX10L and IRX14. *The Plant Journal*, n/a-n/a.
779 Nieduszynski, I., & Marchessault, R. H. (1971). Structure of β-D-(1-4) xylan hydrate. *Nature*
780 *(London)*, 232(5305), 46-47.
781 Nieduszynski, I. A., & Marchessault, R. H. (1972). Structure of β,D(1-4')-xylan hydrate.
782 *Biopolymers*, 11(7), 1335-1344.
783 Nishiyama, Y., Langan, P., & Chanzy, H. (2002). Crystal structure and hydrogen-bonding
784 system in cellulose Iβ from synchrotron X-ray and neutron fiber diffraction. *J. Am.*
785 *Chem. Soc.*, 124(31), 9074-9082.
786 Ordaz-Ortiz, J. J., Marcus, S. E., & Knox, J. P. (2009). Cell wall microstructure analysis
787 implicates hemicellulose polysaccharides in cell adhesion in tomato fruit pericarp
788 parenchyma. *Molecular Plant,* 2, 910-921.

Pawar, P. M., Derba-Maceluch, M., Chong, S. L., Gomez, L. D., Miedes, E., Banasiak, A., . . . Mellerowicz, E. J. (2016). Expression of fungal acetyl xylan esterase in Arabidopsis thaliana improves saccharification of stem lignocellulose. *Plant Biotechnol J,* 14(1), 387-397.

Pawar, P. M.-A., Derba-Maceluch, M., Chong, S.-L., Gandla, M. L., Bashar, S. S., Sparrman, T., . . . Mellerowicz, E. J. (2017). In muro deacetylation of xylan affects lignin properties and improves saccharification of aspen wood. *Biotechnology for Biofuels,* 10.

Quemener, B., Vigouroux, J., Rathahao, E., Tabet, J. C., Dimitrijevic, A., & Lahaye, M. (2015). Negative electrospray ionization mass spectrometry: a method for sequencing and determining linkage position in oligosaccharides from branched hemicelluloses. *Journal of Mass Spectrometry,* 50, 247-264.

Ralet, M. C., Williams, M. A. K., Tanhatan-Nasseri, A., Ropartz, D., Quemener, B., & Bonnin, E. (2012). Innovative Enzymatic Approach to Resolve Homogalacturonans Based on their Methylesterification Pattern. *Biomacromolecules,* 13(5), 1615-1624.

Rappe, A. K., Casewit, C. J., Colwell, K. S., Goddard, W. A., III, & Skiff, W. M. (1992). UFF, a full periodic table force field for molecular mechanics and molecular dynamics simulations. *J. Am. Chem. Soc.,* 114(25), 10024-10035.

Rappe, A. K., & Goddard, W. A., III. (1991). Charge equilibration for molecular dynamics simulations. *J. Phys. Chem.,* 95(8), 3358-3363.

Ray, S., Vigouroux, J., Quemener, B., Bonnin, E., & Lahaye, M. (2014). Novel and diverse fine structures in LiCl-DMSO extracted apple hemicelluloses. *Carbohydrate Polymers,* 108, 46-57.

812 Revol, J. F., Bradford, H., Giasson, J., Marchessault, R. H., & Gray, D. G. (1992). Helicoidal
813 self-ordering of cellulose microfibrils in aqueous suspension. *International Journal of*
814 *Biological Macromolecules,* 14(3), 170-172.
815 Rojas, O. J. (2016). *Cellulose Chemistry and Properties: Fibers, Nanocelluloses and*
816 *Advanced Materials*: Springer.
817 Sauerbrey, G. (1959). *Z. Phys.,* 155, 206.
818 Scheller, H. V., & Ulvskov, P. (2010). Hemicelluloses. *Annual Review of Plant Biology,*
819 61(1), 263-289.
820 Sims, I. M., Craik, D. J., & Bacic, A. (1997). Structural characterisation of
821 galactoglucomannan secreted by suspenstion-cultured cells of *Nicotiana*
822 *plumbaginifolia*. *Carbohydrate Research,* 303, 79-92.
823 Takizawa, A., Hyodo, H., Wada, K., Ishii, T., Satoh, S., & Iwai, H. (2014). Regulatory
824 specialization of xyloglucan (XG) and glucuronoarabinoxylan (GAX) in pericarp cell
825 walls during fruit ripening in tomato (Solanum lycopersicum). *Plos One,* 9, e89871.
826 Teleman, A., Larsson, P. T., & Iversen, T. (2001). On the accessibility and structure of xylan
827 in birch kraft pulp. *Cellulose,* 8(3), 209-215.
828 Thibault, J. F. (1979). Automatisation du dosage des substances pectiques par laméthode au
829 meta-hydroxydiphenyl. *Lebensmittel-Wissenschaft & Technologie,* 12, 247–251.
830 Tollier, M. T., & Robin, J. P. (1979). Adapation de la méthode à l'orcinol-sulfurique au
831 dosage automatique des glucides neutres totaux: Conditionsd'application aux extraits
832 d'origine végétale. *Annals des Technologies agricoles,* 28, 1-15.
833 Verlet, L. (1967). Computer "experiments" on classical fluids. I. Thermodynamical properties
834 of Lennard-Jones molecules. *Phys. Rev.,* 159(1), 98-103.

Villares, A., Bizot, H., Moreau, C., Rolland-Sabate, A., & Cathala, B. (2017). Effect of xyloglucan molar mass on its assembly onto the cellulose surface and its enzymatic susceptibility. *Carbohydrate Polymers*, 157, 1105-1112.

Villares, A., Moreau, C., Capron, I., & Cathala, B. (2014). Chitin Nanocrystal-Xyloglucan Multilayer Thin Films. *Biomacromolecules*, 15(1), 188-194.

Villares, A., Moreau, C., Dammak, A., Capron, I., & Cathala, B. (2015). Kinetic aspects of the adsorption of xyloglucan onto cellulose nanocrystals. *Soft Matter*, 11(32), 6472-6481.

Voragen, F., Schols, H., & Visser, R. (2003). Advances in pectin and pectinase research. *Annals of Botany*, 94, 479-480.

York, W. S., Oates, J. E., van Halbeek, H., Darvill, A., & Albersheim, P. (1988). Location of the *O*-acetyl substituents on a nonasaccharide repeating unit of sycamore extracellular xyloglucan. *Carbohydrate Research*, 173, 113-132.

Yuan, Y., Teng, Q., Zhong, R., & Ye, Z. H. (2016). Roles of Arabidopsis TBL34 and TBL35 in xylan acetylation and plant growth. *Plant Sci*, 243, 120-130.